Synthesis and initial PET imaging of new potential dopamine D3 receptor radioligands (E)-4,3,2-[11C]methoxy-N-4-(4-(2-methoxyphenyl)piperazin-1-yl)butyl-cinnamoylamides

ARTICLE *in* BIOORGANIC & MEDICINAL CHEMISTRY · NOVEMBER 2005

Impact Factor: 2.79 · DOI: 10.1016/j.bmc.2005.06.055 · Source: PubMed

4 AUTHORS, INCLUDING:

Bruce Mock
Indiana University-Purdue University India…
83 PUBLICATIONS **1,998** CITATIONS
SEE PROFILE

Qi-Huang Zheng
Indiana University-Purdue University Scho…
125 PUBLICATIONS **1,887** CITATIONS
SEE PROFILE

Available online at www.sciencedirect.com
SCIENCE DIRECT®
Bioorganic & Medicinal Chemistry 13 (2005) 6233–6243
Bioorganic & Medicinal Chemistry

Synthesis and initial PET imaging of new potential dopamine D_3 receptor radioligands (*E*)-4,3,2-[^{11}C]methoxy-*N*-4-(4-(2-methoxyphenyl)piperazin-1-yl)butyl-cinnamoylamides

Mingzhang Gao, Bruce H. Mock, Gary D. Hutchins and Qi-Huang Zheng*

Department of Radiology, Indiana University School of Medicine, 1345 West 16th Street, L-3 Room 202, Indianapolis, IN 46202, USA

Received 2 June 2005; revised 23 June 2005; accepted 23 June 2005
Available online 8 August 2005

Abstract—D_3 receptor radioligands (*E*)-4,3,2-[^{11}C]methoxy-*N*-4-(4-(2-methoxyphenyl)piperazin-1-yl)butyl-cinnamoylamides (4-[^{11}C]MMC, [^{11}C]**1a**; 3-[^{11}C]MMC, [^{11}C]**1b**; and 2-[^{11}C]MMC, [^{11}C]**1c**) were synthesized for evaluation as novel potential positron emission tomography (PET) imaging agents for brain D_3 receptors. The new tracers 4,3,2-[^{11}C]MMCs were prepared by *O*-[^{11}C]methylation of corresponding precursors (*E*)-4,3,2-hydroxy-*N*-4-(4-(2-methoxyphenyl)piperazin-1-yl)butyl-cinnamoylamides (4,3,2-HMCs) using [^{11}C]methyl triflate and isolated by the solid-phase extraction (SPE) purification procedure with 40–65% radiochemical yields, decay corrected to end of bombardment (EOB), and a synthesis time of 15–20 min. The PET dynamic studies of the tracers [^{11}C]**1a–c** in rats were performed using an animal PET scanner, IndyPET-II, developed in our laboratory. The results show that the brain uptake sequence was 4-[^{11}C]MMC > 3-[^{11}C]MMC > 2-[^{11}C]MMC, which is consistent with their in vitro biological properties. The initial PET blocking studies of the tracers 4,3,2-[^{11}C]MMCs with corresponding pretreatment drugs (*E*)-4,3,2-methoxy-*N*-4-(4-(2-methoxyphenyl)piperazin-1-yl)butyl-cinnamoylamides (4,3,2-MMCs, **1a–c**) had no effect on 4,3,2-[^{11}C]MMCs-PET rat brain imaging. These results suggest that the localization of 4,3,2-[^{11}C]MMCs in rat brain is mediated by nonspecific processes, and the visualization of 4,3,2-[^{11}C]MMCs-PET in rat brain is related to nonspecific binding.

1. Introduction

The neurotransmitter dopamine is implicated in a number of physiological and pathophysiological processes, which regulate brain functions like motion, emotion, and cognition.[1] Five subtypes of brain dopamine receptors have been classified into two major classes: the $D_{1\text{-like}}$ receptors including D_1 and D_5 receptors and $D_{2\text{-like}}$ receptors including D_2, D_3, and D_4 receptors. The dopamine $D_{2\text{-like}}$ receptor subtypes, D_2 and D_3 receptors, are recognized as potential therapeutic targets for the treatment of various neurological and psychiatric disorders such as Parkinson's disease, Huntington's disease, and schizophrenia.[2] An in vivo biomedical imaging technique, positron emission tomography (PET), coupled with appropriate receptor radioligands, has become a clinically valuable and accepted diagnostic tool to image brain diseases.[3] The dopamine $D_{2\text{-like}}$ receptor was the first neuroreceptor to be visualized by PET with the tracer 3-*N*-[^{11}C]methylspiperone ([^{11}C]NMSP).[4] There is a growing interest in developing positron-labeled D_2 and D_3 receptor antagonists as in vivo markers for use in PET, and many attempts have been made in this area.[5–7] However, so far only [^{11}C]raclopride has been extensively used in human clinical PET studies, because of its high affinity and great specificity for binding to cerebral dopaminergic D_2 receptors.[8] We have developed an improved synthetic approach for the production of [^{11}C]raclopride routinely used in our PET center for human and animal studies,[9,10] and we are interested in the development of PET D_3 receptor radioligands. (*E*)-4,2-Methoxy-*N*-4-(4-(2-methoxyphenyl)piperazin-1-yl)butyl-cinnamoylamides (4-MMC, **1a**, K_i/D_3 0.38 nM, K_i/D_2 12 nM, ratio D_2/D_3 32; 2-MMC, **1c**, K_i/D_3 0.56 nM, K_i/D_2 14 nM, ratio D_2/D_3 25) are two new high-affinity D_3 receptor antagonists recently developed by Hackling et al.[1] Both compounds possess the combination of favorable pharmacokinetics and nanomolar K_i binding affinity for D_3 receptor, and *O*-methyl positions amenable to labeling with carbon-11. These same properties are often beneficial in a diagnostic radiotracer. We investigated whether ^{11}C-labeled analogs of 4-MMC and 2-MMC, (E)-4,2-[^{11}C]methoxy-*N*-4-(4-

Keywords: (*E*)-4,3,2-[^{11}C]Methoxy-*N*-(4-4-(2-methoxyphenyl)butyl-cinnamoylamides; Radioligands; Positron emission tomography; Brain; D_3 receptors.
* Corresponding author. Tel.: +1 317 278 4671; fax: +1 317 278 9711; e-mail: qzheng@iupui.edu

0968-0896/$ - see front matter © 2005 Elsevier Ltd. All rights reserved.
doi:10.1016/j.bmc.2005.06.055

(2-methoxyphenyl)piperazin-1-yl)butyl)-cinnamoylamides (4-[^{11}C]MMC, [^{11}C]**1a**; 2-[^{11}C]MMC, [^{11}C]**1c**), could be used to map brain D_3 receptors in vivo. As part of our efforts to evaluate potential brain-imaging agents, we synthesized 4-[^{11}C]MMC ([^{11}C]**1a**); (E)-3-[^{11}C]methoxy-*N*-4-(4-(2-methoxyphenyl)piperazin-1-yl)butyl-cinnamoylamide (3-[^{11}C]MMC, [^{11}C]**1b**); and 2-[^{11}C]MMC ([^{11}C]**1c**), and performed initial PET imaging studies of the tracers [^{11}C]**1a**–**c** in rat brain.

2. Results and discussion

2.1. Chemistry, radiochemistry, and lipophilicity

The synthetic approach for 4,3,2-[^{11}C]MMCs ([^{11}C]**1a**–**c**) is shown in Scheme 1.

The synthesis of the precursors (*E*)-4,3,2-hydroxy-*N*-4-(4-(2-methoxyphenyl)piperazin-1-yl)butyl-cinnamoylamides (4,3,2-HMCs, **1d**–**f**), and reference standards (*E*)-4,3,2-methoxy-*N*-4-(4-(2-methoxyphenyl)piperazin-1-yl)butyl-cinnamoylamides (4,3,2-MMCs, **1a**–**c**), as indicated in Scheme 1, was performed using a modification of the literature procedure.[1] Commercially available *N*-(4-bromobutyl)phthalimide (**2**) was reacted with 1-(2-methoxyphenyl)piperazine (**3**) to give an intermediate (4-(4-(2-methoxyphenyl)piperazin-1-yl)butyl)phthalimide (**4**), which was used for next step reaction without further purification. The intermediate **4** was reacted with hydrazine hydrate to provide 4-(4-(2-methoxyphenyl)piperazin-1-yl)butylamine (**5**) in 92% yield. There were two methods to prepare the precursors and reference standards. Method A: 4,3,2-methoxycinnamic acids (**6a**–**c**) and 4,3,2-hydroxycinnamic acids (**6d**–**f**)

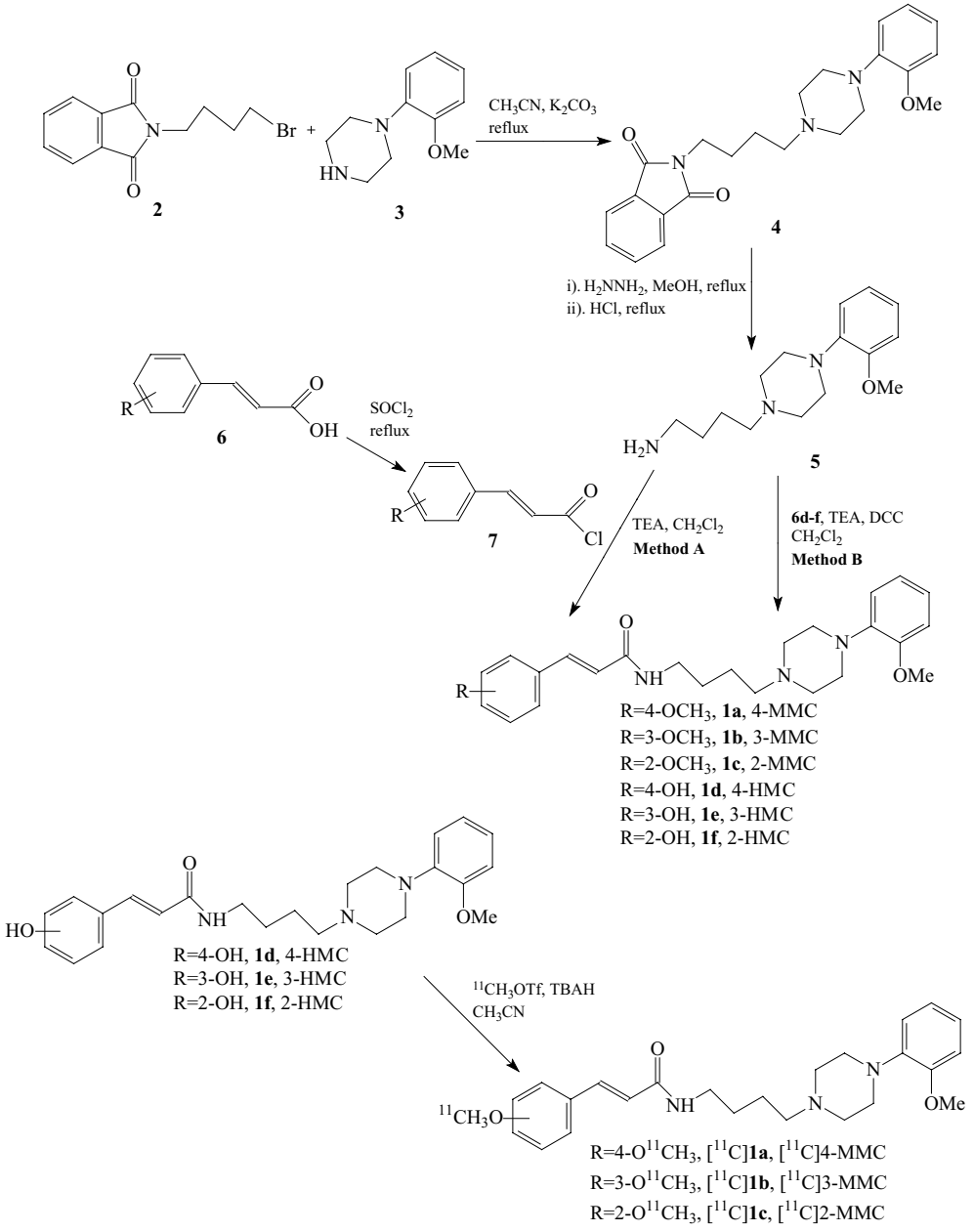

Scheme 1. Synthetic approach for the tracers 4,3,2-[^{11}C]MMCs ([^{11}C]**1a**–**c**).

were treated with thionyl chloride to produce corresponding 4,3,2-methoxycinnamoyl chlorides (**7a–c**) and 4,3,2-hydroxycinnamoyl chlorides (**7d–f**), which were reacted with compound **5** in triethylamine (TEA) and dichloromethane to give the reference standards **1a–c** and precursors **1d–f** for radiolabeling. Method B: Compounds **6d–f** were directly reacted with compound **5** in TEA and 1,3-dicyclohexylcarbodiimide (DCC) to afford the precursors **1d–f**. The chemical yields of the reference standards using Method A are moderate, and the chemical yields of the precursors using Method B are higher than using Method A.

The precursors **1d–f** were labeled by [^{11}C]methyl triflate[11] through *O*-[^{11}C]methylation[12] under basic conditions using tetrabutylammonium hydroxide (TBAH) to give the target tracers 4,3,2-[^{11}C]MMCs ([^{11}C]**1a–c**). The tracers were isolated by solid-phase extraction (SPE) purification.[13] The radiochemical yields for target tracers [^{11}C]**1a–c** were 40–65%, based on $^{11}CO_2$, decay corrected to end of bombardment (EOB). The synthesis time of the tracers was 15–20 min. The large polarity difference between the precursors and the labeled methylated products permitted the use of SPE technique for rapid purification of labeled products from the radiolabeling reaction mixture. The reaction mixture was diluted with $NaHCO_3$ and loaded onto C-18 cartridge by gas pressure. The cartridge column was washed with water to remove unreacted [^{11}C]methyl triflate, its precursor, and reaction solvent. The final labeled product was then eluted with ethanol. Chemical purity, radiochemical purity, and specific radioactivity were determined by analytical reversed-phase HPLC methods. The chemical purities of precursors **1d–f** and reference standards **1a–c** were >95%. The radiochemical purities of target radiotracers [^{11}C]**1a–c** were >99%, and the chemical purities of target radiotracers [^{11}C]**1a–c** were >93%. The specific radioactivity of target radiotracers [^{11}C]**1** and [^{11}C]**2** was >1 Ci/μmol at end of synthesis (EOS). Retention times in the analytical HPLC system were: t_R **1d** = 4.13 min, t_R **1e** = 3.74 min, t_R **1f** = 3.46 min; t_R [^{11}C]**1a** = 6.75 min, t_R [^{11}C]**1b** = 6.48 min, t_R [^{11}C]**1c** = 6.05 min.

The ability of a D_3 receptor radioligand to penetrate the blood–brain barrier (BBB) could be due, at least in part, to its lipophilicity, and thus we were interested in identifying an analog that was significantly lipophilic brain tracer. We calculated lipophilicity coefficients (log *P*) of the tracers 4,3,2-[^{11}C]MMCs based on their retention times that were measured by C-18 HPLC method.[14] The calculation results showed that the log *P* values of the tracers 4,3,2-[^{11}C]MMCs are 2.86, 2.81, and 2.71, respectively, that is, the lipophilicity sequence is 4-[^{11}C]MMC > 3-[^{11}C]MMC > 2-[^{11}C]MMC. Therefore, we assume the ability to penetrate the BBB is 4-[^{11}C]MMC > 3-[^{11}C]MMC > 2-[^{11}C]MMC, and 4-[^{11}C]MMC is the most promising candidate for use as a potential brain imaging agent in a series of 4,3,2-[^{11}C]MMCs compounds.

2.2. In vivo PET imaging studies

In vivo dynamic PET imaging studies[15] of the tracers 4,3,2-[^{11}C]MMCs in young adult female Sprague–Dawley rats were performed in the IndyPET-II scanner[16] for 60 min post iv injection of 0.5–1.0 mCi of the tracer in a rat, and the images are shown in Figures 1–3. All PET

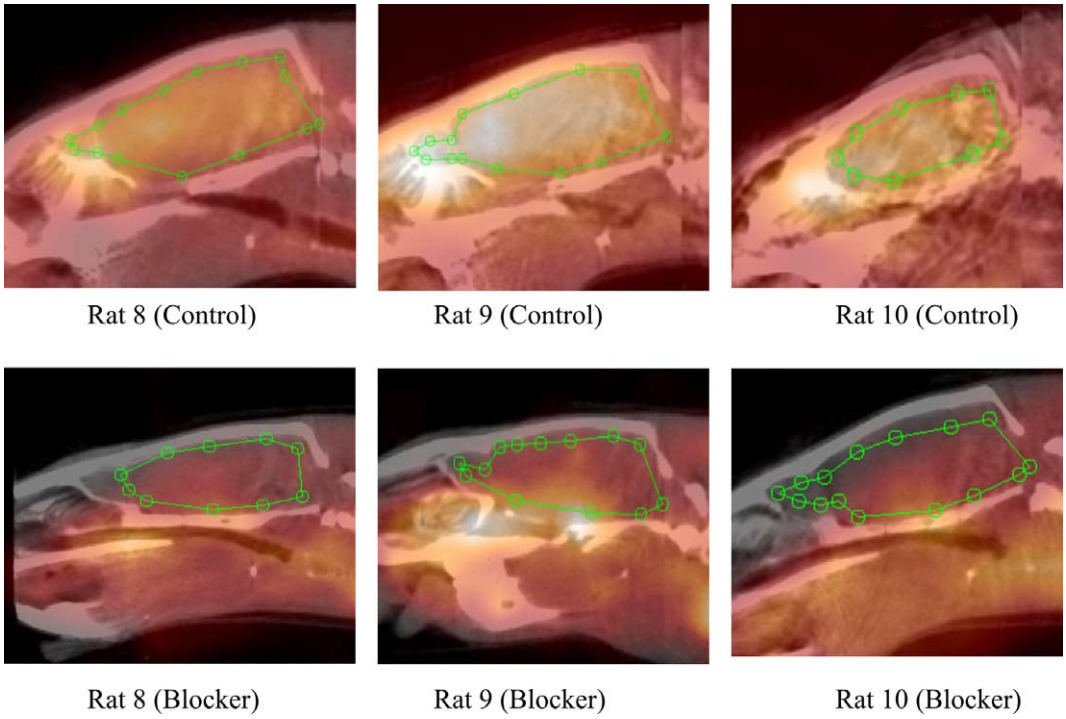

Figure 1. PET/CT overlay images of the tracer 4-[^{11}C]MMC with no blocker (control) and with blocker 4-MMC (3.0 mg/kg) (blocker) in female rats anesthetized with acepromazine (0.2 mg/kg, i.m.) and torbugesic (0.2 mg/kg, i.m.), administrated with 0.5–1.0 mCi radioactivity, and scanned with IndyPET-II for 60 min. The images are sagittal views in which the location of the brain is indicated in the circle region.

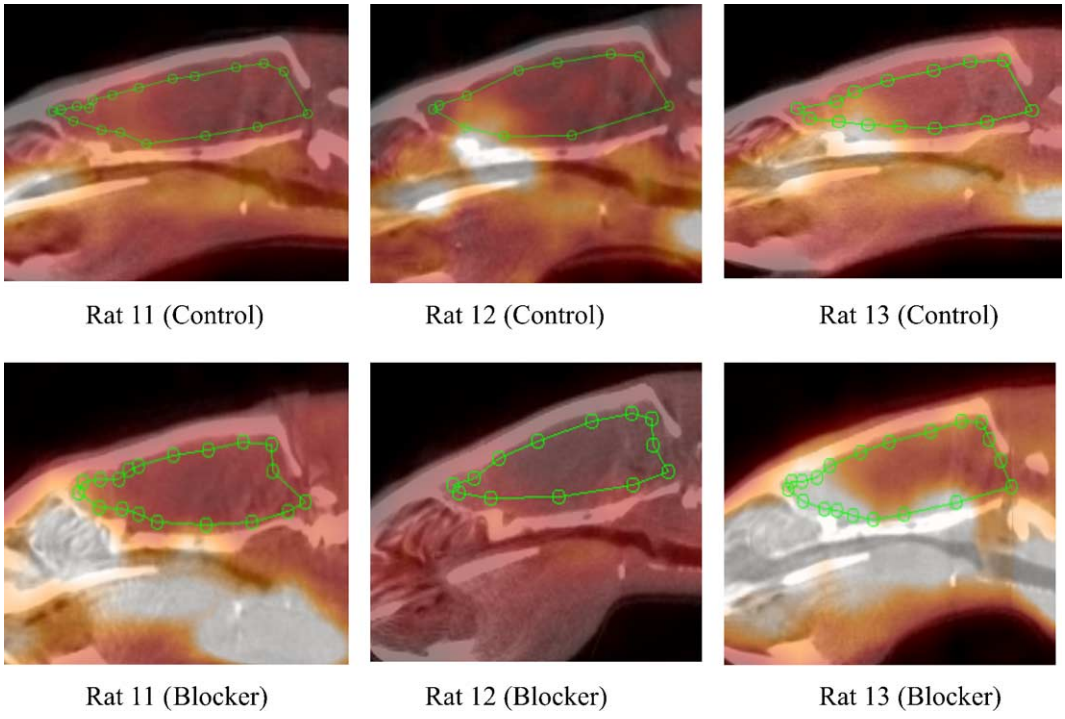

Figure 2. PET/CT overlay images of the tracer 3-[^{11}C]MMC with no blocker (control) and with blocker 3-MMC (3.0 mg/kg) (blocker) in female rats anesthetized with acepromazine (0.2 mg/kg, i.m.) and torbugesic (0.2 mg/kg, i.m.), administrated with 0.5–1.0 mCi radioactivity, and scanned with IndyPET-II for 60 min. The images are sagittal views in which the location of the brain is indicated in the circle region.

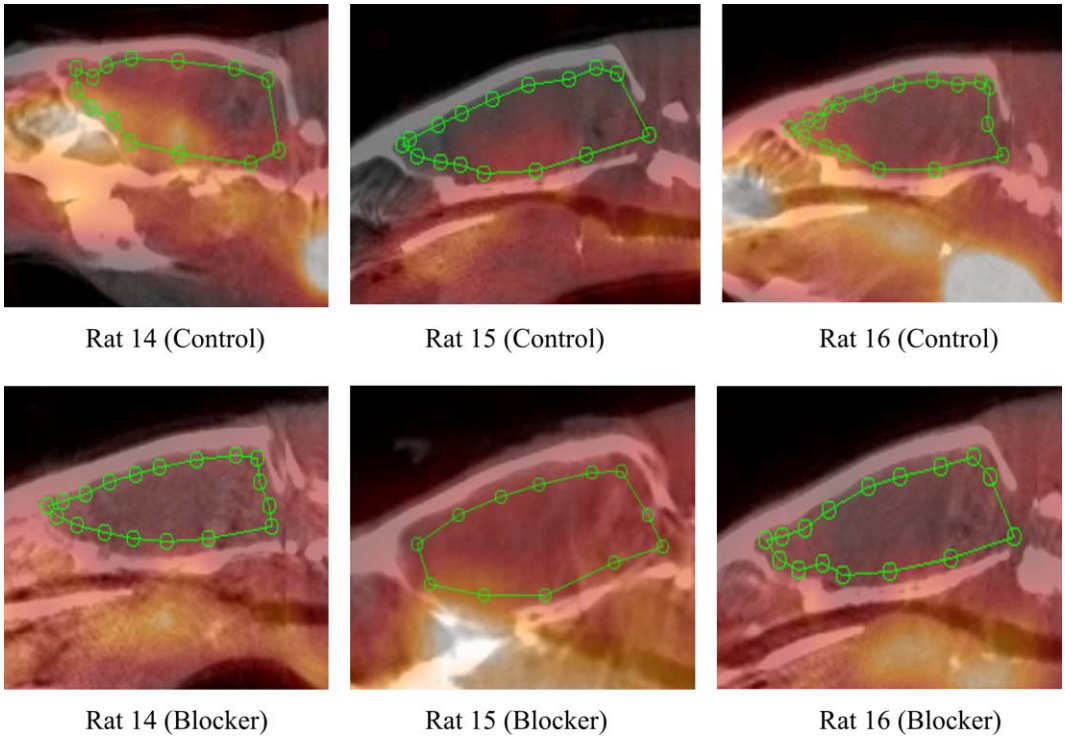

Figure 3. PET/CT overlay images of the tracer 2-[^{11}C]MMC with no blocker (control) and with blocker 2-MMC (3.0 mg/kg) (blocker) in female rats anesthetized with acepromazine (0.2 mg/kg, i.m.) and torbugesic (0.2 mg/kg, i.m.), administrated with 0.5–1.0 mCi radioactivity, and scanned with IndyPET-II for 60 min. The images are sagittal views in which the location of the brain is indicated in the circle region.

images are sagittal views and overlaid with μ-CT. The location of the brain is indicated in the circle region. We have developed a method[17] for registration and fusion of small animal scans acquired with the IndyPET-II scanner and the EVS RS-9 CT scanner (Enhanced Vision System, London, Ontario), which can

provide vital information about the anatomic information of tissues and organs in small animals. The μ-CT uses X-rays that pass through the animal to obtain structural information of the animal. It is an ideal instrument for biomedical research laboratories to nondestructively acquire 3-D images of both in vivo and in vitro specimens. The X-ray radiation that is imposed on the animal is minimum and does not result in any physiology change. The registration and fusion of EVS μ-CT with IndyPET-II will help to draw the regions of interest (ROIs) of the images. All images were acquired in list-mode and sorted into 15×20-s frames, 10×60-s frames, and 9×300-s frames. Images were reconstructed using filtered back projection with a 70% Hanning filter (4.242 cm^{-1} cutoff frequency). The PET/CT images of the tracer 4-[^{11}C]MMC from rats 8 to 10 in Figure 1 showed that some brain images are visible with the tracer, and some images are not clear. This situation applied to the PET/CT images of the tracer 3-[^{11}C]MMC from rats 11 to 13 in Figure 2 and the PET/CT images of the tracer 2-[^{11}C]MMC from rats 14 to 16 in Figure 3. Comparing the images of the tracers 4,3,2-[^{11}C]MMCs in Figures 1–3, we assume the brain uptake sequence was 4-[^{11}C]MMC > 3-[^{11}C]MMC > 2-[^{11}C]MMC.

In vivo competitive inhibition studies were performed to assess the in vivo specificity of 4,3,2-[^{11}C]MMCs to brain D_3 receptors and whether the tracer distribution is susceptible to indirect pharmacological or pharmacodynamic effects that could complicate uptake site measurements. Competition or 'blocking' study was carried out by pretreating groups of animals with drugs, unlabeled D_3 receptor antagonists, which compete, or are believed to compete for the same binding site that tracer interacts with in the animal brain. For the blocking imaging studies,[15] the rats were pretreated by intraperitoneal injection with the drugs 4,3,2-MMCs prior to intravenous injection with corresponding tracers 4,3,2-[^{11}C]MMCs. The blocking images with blockers 4,3,2-MMCs are shown in Figures 1–3. Similarly, the blocking studies show that some of the PET/CT brain images of the tracers 4,3,2-[^{11}C]MMCs with corresponding blockers 4,3,2-MMCs from rats 8 to 16 were visible, and some brain images were not clear as indicated in Figures 1–3. In comparison of the brain images in the blocking studies with those in control studies shows that the changes are no distinct. Therefore, we assume there is not significant difference between control studies and blocking studies.

The dynamic PET data of the tracers 4-[^{11}C]MMC with no blocker (control) and with blockers 4-MMC (blocker) are shown in Figures 4 and 5. The plot in Figure 4 is the individualized average brain ROI intensity (y-axis) versus time (x-axis) from injection, which indicated the kinetics of the tracer 4-[^{11}C]MMC in each individual animal rats 8, 9, and 10 at each time point in 60 min of the entire scan time. The plot in Figure 5 is the comparison of the accumulated average intensity values (y-axis) between 4-[^{11}C]MMC with no blocker (control) and 4-[^{11}C]MMC with blocker 4-MMC (blocker) in two different experimental animal groups ($n = 3$) (x-axis) in 60 min of the entire scan time, which showed that the tracer 4-[^{11}C]MMC uptake in the brain was changed in the blocking study. However, a t-test comparing the means of 4-[^{11}C]MMC with no blocker and with blocker 4-MMC gave a P-value of 0.31, which did not denote the presence of a statistically significant difference. Therefore, we conclude that there was no significant blocking in the data set, the uptakes of 4-[^{11}C]MMC in rat brain might be the result of nonspecific binding, and the visualization of 4-[^{11}C]MMC-PET on rat brain is associated with nonspecific binding.

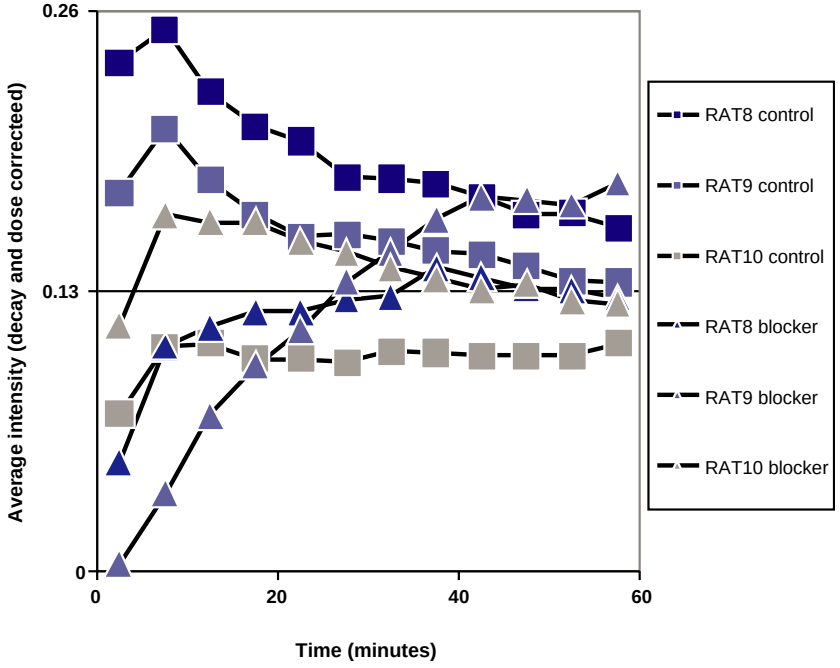

Figure 4. The kinetics of the tracer 4-[^{11}C]MMC in each rat brain with no blocker (control) and with blocker 4-MMC (blocker) showed the individualized average brain region of interest intensity versus time from injection in 60 min of entire scan time.

Similarly, the dynamic PET data of the tracer 3-[^{11}C]MMC with no blocker (control) and with blocker 3-MMC (blocker) are shown in Figures 6 and 7. The plot in Figure 6 is the individualized average brain ROI intensity (y-axis) versus time (x-axis) from injection, which indicated the kinetics of the tracer 3-[^{11}C]MMC in each individual animal rats 11, 12, and 13 at each time point in 60 min of the entire scan time. The plot in Figure 7 is the comparison of the accumulated average intensity values (y-axis) between 3-[^{11}C]MMC with no blocker (control) and 3-[^{11}C]MMC with blocker 3-MMC (blocker) in two different experimental animal groups ($n = 3$) (x-axis) in 60 min of the entire scan time, which showed that the tracer 3-[^{11}C]MMC uptake in the brain was changed in the blocking study. However, a t-test comparing the means of 3-[^{11}C]MMC with no blocker and with blocker 3-MMC gave a P value of 0.79, which did not denote the presence of a statistically significant difference. Therefore, we conclude that there was no significant blocking in the data set, the uptakes of 3-[^{11}C]MMC in rat brain might be the result of nonspecific binding, and the visualization of 3-[^{11}C]MMC-PET on rat brain is associated with nonspecific binding.

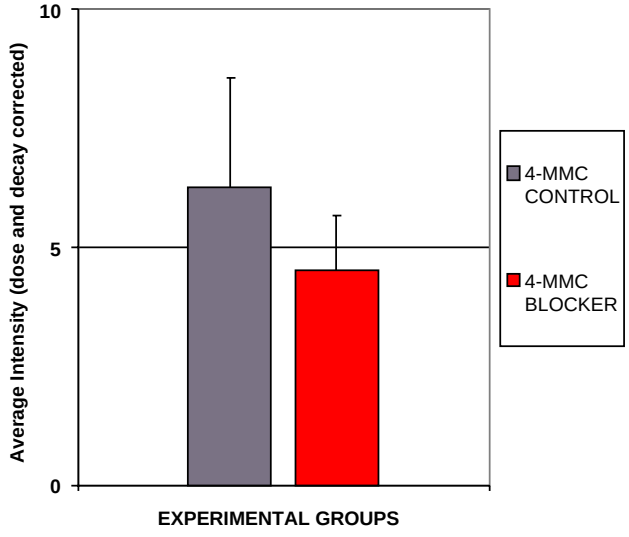

Figure 5. Comparison of the tracer 4-[^{11}C]MMC uptake in rat brain in the absence and presence of blocker 4-MMC (control group and blocker group).

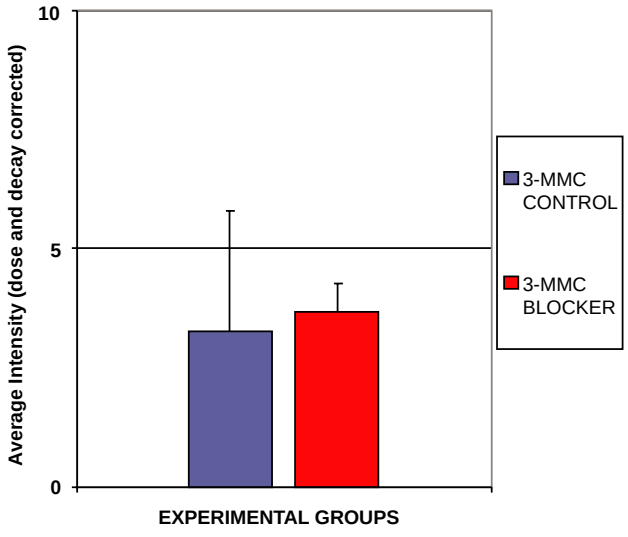

Figure 7. Comparison of the tracer 3-[^{11}C]MMC uptake in rat brain in the absence and presence of blocker 3-MMC (control group and blocker group).

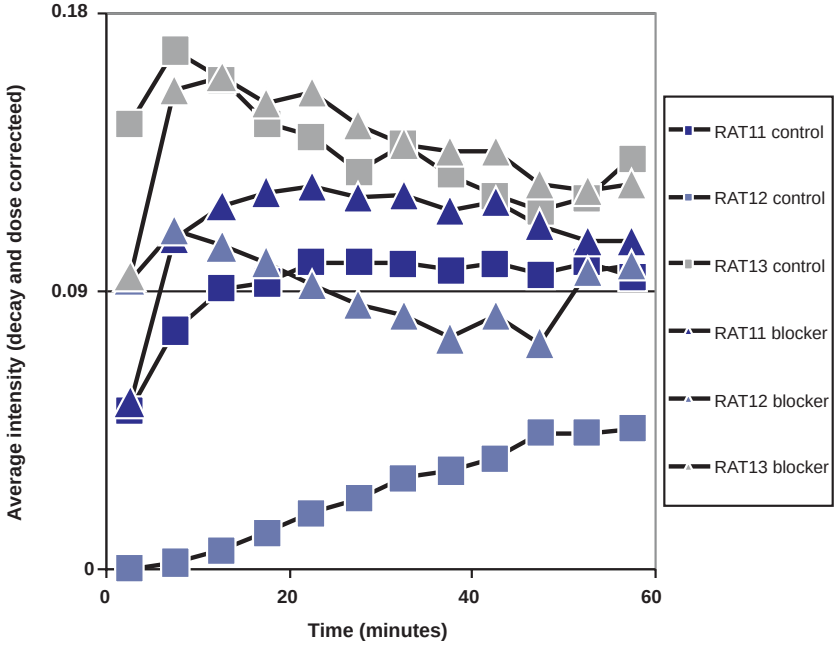

Figure 6. The kinetics of the tracer 3-[^{11}C]MMC in each rat brain with no blocker (control) and with blocker 3-MMC (blocker) showed the individualized average brain region of interest intensity versus time from injection in 60 min of entire scan time.

Likewise, the dynamic PET data of the tracer 2-[^{11}C]MMC with no blocker (control) and with blocker 2-MMC (blocker) are shown in Figures 8 and 9. The plot in Figure 8 is the individualized average brain ROI intensity (*y*-axis) versus time (*x*-axis) from injection, which indicated the kinetics of the tracer 2-[^{11}C]MMC in each individual animal rats 14, 15, and 16 at each time point in 60 min of the entire scan time. The plot in Figure 9 is the comparison of the accumulated average intensity values (*y*-axis) between 2-[^{11}C]MMC with no blocker (control) and 2-[^{11}C]MMC with blocker 2-MMC (blocker) in two different experimental animal groups ($n = 3$) (*x*-axis) in 60 min of the entire scan time, which showed that the tracer 2-[^{11}C]MMC uptake in the brain was changed in the blocking study. However, a *t*-test comparing the means of 2-[^{11}C]MMC with no blocker and with blocker 2-MMC gave a *P*-value of 0.29, which did not denote the presence of a statistically significant difference. Therefore, we conclude that there was no significant blocking in the data set, the uptakes of 2-[^{11}C]MMC in rat brain might be the result of nonspecific binding, and the visualization of 2-[^{11}C]MMC-PET on rat brain is associated with nonspecific binding.

The comparison of the accumulated average intensity in rat brain in the tracers 4,3,2-[^{11}C]MMCs in three different experimental animal groups (control) in 60 min of the entire scan time is shown in Figure 10. A *t*-test comparing the means of 4-[^{11}C]MMC with 3-[^{11}C]MMC, 4-[^{11}C]MMC with 2-[^{11}C]MMC, and 3-[^{11}C]MMC with 2-[^{11}C]MMC gave a *P*-value of 0.20, 0.12, and 0.72, respectively, which did not denote the presence of a statistically significant difference. From Figure 10, the brain uptake sequence was 4-[^{11}C]MMC > 3-[^{11}C]MMC > 2-[^{11}C]MMC, which is consistent with their in vitro biological properties (4-MMC, K_i/D_3 0.38 nM, K_i/D_2 12 nM, ratio D_2/D_3 32; 3-MMC, N/A; and 2-MMC, K_i/D_3 0.56 nM, K_i/D_2 14 nM, ratio D_2/D_3 25) that 4-MMC is the most potent D_3 receptor antagonist in 4,3,2-MMCs.[1] The previously described lipophilicity information also partially accounts for this in vivo imaging result, since the ability to penetrate the BBB is 4-[^{11}C]MMC > 3-[^{11}C]MMC > 2-[^{11}C]MMC. A more likely explanation is difference in metabolism of 4,3,2-[^{11}C]MMCs. The ease of metabolism with *O*-demethylation mechanism[18] for 4,3,2-[^{11}C]MMCs is 2-[^{11}C]MMC > 3-[^{11}C]MMC > 4-[^{11}C]MMC as indicated in Figure 11, therefore, 2-[^{11}C]MMC appears to have a

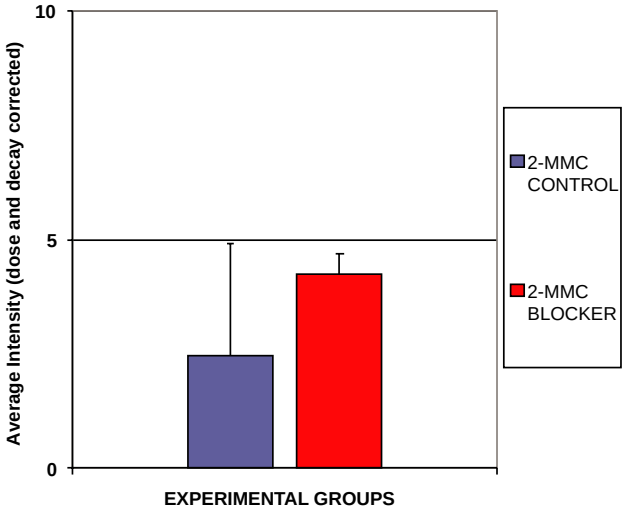

Figure 9. Comparison of the tracer 2-[^{11}C]MMC uptake in rat brain in the absence and presence of blocker 2-MMC (control group and blocker group).

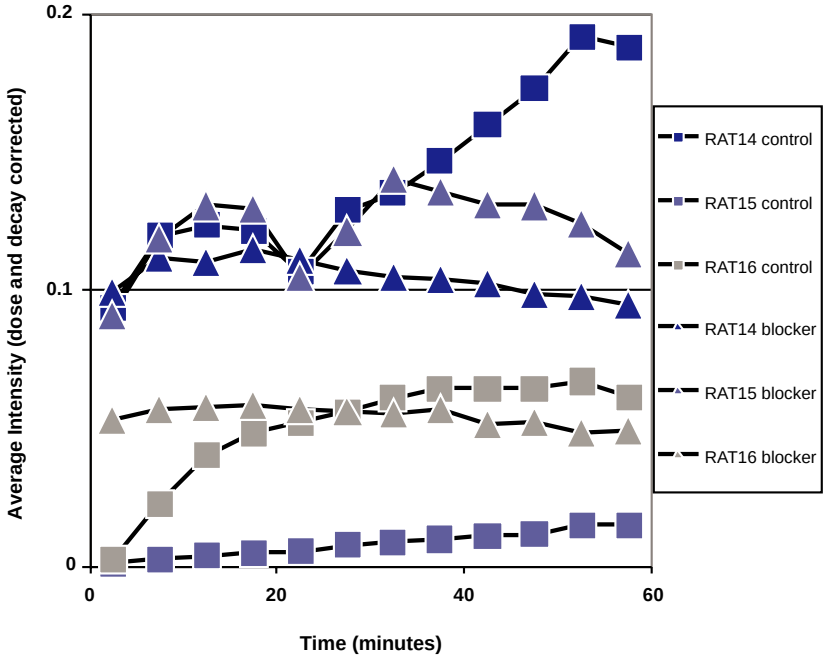

Figure 8. The kinetics of the tracer 2-[^{11}C]MMC in each rat brain with no blocker (control) and with blocker 2-MMC (blocker) showed the individualized average brain region of interest intensity versus time from injection in 60 min of entire scan time.

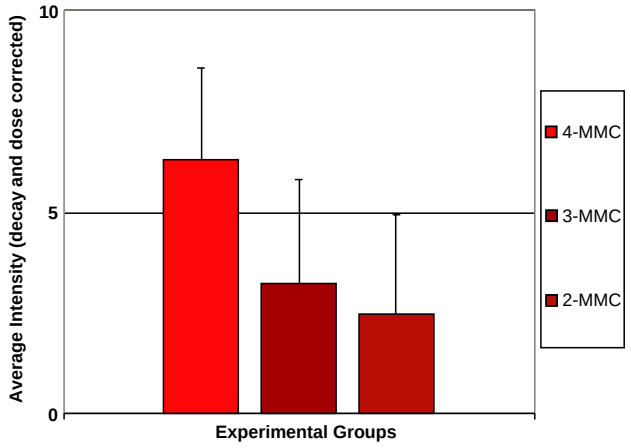

Figure 10. Comparison of the tracers 4,3,2-[^{11}C]MMCs uptake in rat brain in control groups.

faster washout without longer retention in the rat brain than does 3-[^{11}C]MMC and 4-[^{11}C]MMC.

3. Conclusion

The synthetic procedures that provide new tracers 4,3,2-[^{11}C]MMCs have been well developed. The initial PET imaging studies of the tracers 4,3,2-[^{11}C]MMCs showed that these three tracers had a certain uptake in the rat brain. Comparative studies of the images and the average intensity in the rat brain of 4,3,2-[^{11}C]MMCs showed the brain uptake sequence was 4-[^{11}C]MMC > 3-[^{11}C]MMC > 2-[^{11}C]MMC. However, the results from the blocking studies by intraperitoneal injection with pretreatment drugs 4,3,2-MMCs prior to intravenous injection with corresponding tracers 4,3,2-[^{11}C]MMCs showed that no specific binding is present in all of the three tracers. These results suggest that localization of 4,3,2-[^{11}C]MMCs in rat brain is mediated by non-specific processes, and the visualization of 4,3,2-[^{11}C]MMCs-PET in rat brain is related to nonspecific binding.

4. Experimental

4.1. General

All commercial reagents and solvents were used without further purification unless otherwise specified. The [^{11}C]methyl triflate was made according to the literature procedure.[11] Melting points were determined on a MEL-TEMP II capillary tube apparatus and were uncorrected. ^{1}H NMR spectra were recorded on a Bruker QE 300 NMR spectrometer using tetramethylsilane (TMS) as an internal standard. Chemical shift data for the proton resonances were reported in parts per million (δ) relative to the internal standard TMS (δ 0.0). Low-resolution mass spectra (LRMS) were obtained using a Bruker Biflex III MALDI-TOF mass spectrometer, and high-resolution mass spectra (HRMS) measurements were obtained using a Kratos MS80 mass spectrometer, in the Department of Chemistry at Indiana University. Chromatographic solvent proportions are expressed on a volume:volume basis. Thin-layer chromatography was run using Analtech silica gel GF uniplates (5×10 cm^2). Plates were visualized by UV light. Normal phase flash chromatography was carried out on EM Science silica gel 60 (230–400 mesh) with a forced flow of the indicated solvent system in the proportions described below. All moisture-sensitive reactions were performed under a positive pressure of nitrogen maintained by a direct line from a nitrogen source.

Analytical HPLC was performed using a Prodigy (Phenomenex) 5 μm C-18 column, 4.6×250 mm; 3:1:3 CH_3CN–MeOH–20 mM, pH 6.7 $KHPO_4^-$ (buffer solution) mobile phase, flow rate 1.5 mL/min, and UV (240 nm) and γ-ray (NaI) flow detectors. Semi-prep C-18 guard cartridge column 1×1 cm was obtained from E. S. Industries, Berlin, NJ, and part number 300121-C18-BD 10μ. Sterile Millex-GS 0.22 μm vented filter unit was obtained from Millipore Corporation, Bedford, MA.

4.2. Synthesis of precursors and reference standards

4.2.1. 4-(4-(2-Methoxyphenyl)piperazin-1-yl)butylamine (5). A mixture of *N*-(4-bromobutyl)phthalimide (**2**) (21 mmol,

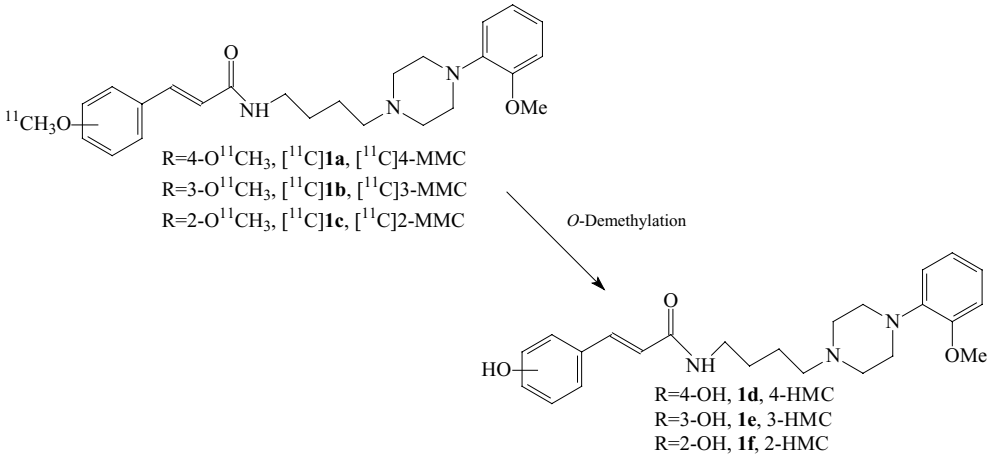

Figure 11. Potential metabolic pathways of the tracers 4,3,2-[^{11}C]MMCs ([^{11}C]**1a**–**c**).

5.92 g), 1-(2-methoxyphenyl)piperazine (**3**) (20 mmol, 3.84 g), and K_2CO_3 (50 mmol, 6.91 g) in acetonitrile or acetone (60 mL) was heated to reflux for 8 h. After further addition of compound **2** (1 mmol, 0.27 g), the mixture was heated for another 4 h. The hot suspension was filtrated and the residue was washed with acetone three times. The filtrates were concentrated under reduced pressure to give an intermediate 4-(4-(2-methoxyphenyl)piperazin-1-yl)butyl)phthalimide (**4**), which was not separated and directly used for next step reaction. Compound **4** (18 mmol, 7.08 g) and hydrazine hydrate (22 mmol, 1.07 g) in methanol (30 mL) were heated to reflux for 2 h. To the hot solution was added 2 N HCl (20 mL), and reflux was continued for another 1 h. After cooling to ambient temperature, the mixture was filtrated and the filtrate was evaporated to dryness. This residue was suspended in water and alkalized with 2 N NaOH. Extraction with ethyl acetate or CH_2Cl_2 yielded compound **5** (4.36 g, 92%) as a low melting point and pure enough white solid, which can be further purified by column chromatography (10:89:1 CH_3OH–CH_2Cl_2–$NH_3{\cdot}H_2O$), R_f = 0.22 (10:89:1 CH_3OH–CH_2Cl_2–$NH_3{\cdot}H_2O$). ^1H NMR (300 MHz, $CDCl_3$): δ 1.25–1.58 (m, 4H, CH_2CH_2), 2.15 (s, 2H, CH_2), 2.43 (t, J = 6.40 Hz, 2H, 1-Pipera-CH_2), 2.67 (s, 4H, Pipera-H), 2.74 (s, 2H, NH_2), 3.10 (s, 4H, Pipera-H), 3.86 (s, 3H, CH_3O), 6.85–7.01 (m, 4H, Ph–H).

4.2.2. General procedure for the preparation of amides (*E*)-4,3,2-methoxy-*N*-4-(4-(2-methoxyphenyl)piperazin-1-yl)butyl-cinnamoylamides (4,3,2-MMCs, 1a–c) and (*E*)-4,3,2-hydroxy-*N*-(4-(4-(2-methoxyphenyl)piperazin-1-yl)butyl)-cinnamoylamides (4,3,2-HMCs, 1d–f). Method A (**1a**–**f**): The 4,3,2-methoxycinnamic acids (**6a**–**c**) or 4,3,2-hydroxycinnamic acids (**6d**–**f**) (0.06 mol) were treated with thionyl chloride (20 mL) and two drops of *N*,*N*-dimethylformamide and then heated at reflux for 2–3 h. The excess thionyl chloride was removed by evaporation under reduced pressure. Residual thionyl chloride was removed by co-evaporation with anhydrous benzene (30 mL) to afford the corresponding 4,3,2-methoxycinnamoyl chlorides (**7a**–**c**) and 4,3,2-hydroxycinnamoyl chlorides (**7d**–**f**). A mixture of compound **5** (2 mmol, 0.526 g), TEA (6 mmol, 0.84 mL), and dry CH_2Cl_2 (15 mL) was cooled down to 0 °C and was stirred under nitrogen for 5 min. Then the corresponding cinnamoyl chloride (**7**) (2.2 mmol) was slowly added and the stirring continued for another 4–15 h. The solvent was removed under reduced pressure. The mixture was added to water and was extracted with CH_2Cl_2. The crude product was purified by silica gel column chromatography (6:94 CH_3OH–CH_2Cl_2) to give pure products **1a**–**f**, R_f = 0.63–0.67 (1:9 CH_3OH–CH_2Cl_2).

Method B (**1d**–**f**): A mixture of 4,3,2-hydroxycinnamic acids (**6d**–**f**) (2 mmol, 0.328 g), TEA (4 mmol, 0.41 g), and compound **5** (2 mmol, 0.526 g) in dry CH_2Cl_2 (25 mL) was stirred at room temperature for 10 min under nitrogen. Then DCC (2.6 mmol, 0.536 g) was added and the stirring continued for another 10–20 h. The mixture was filtrated, and the residue was washed with water. The filtrate was evaporated to dryness, which was purified by column chromatography (6:94 CH_3OH–CH_2Cl_2) to give pure products **1d**–**f**, $R_f \approx 0.63$ (1:9 CH_3OH–CH_2Cl_2).

4.2.2.1. (*E*)-4-Methoxy-*N*-(4-(4-(2-methoxyphenyl)piperazin-1-yl)butyl)-cinnamoylamide (1a). Method A, 78% yield, mp: 137–139 °C. ^1H NMR (300 MHz, $CDCl_3$): δ 1.64 (s, 4H, CH_2CH_2), 2.46 (s, 2H, 1-Pipera-CH_2), 2.68 (s, 4H, Pipera-H), 3.16 (s, 4H, Pipera-H), 3.41 (s, 2H, CH_2CONH), 3.81 (s, 3H, OCH_3), 3.86 (s, 3H, OCH_3), 6.27 (d, J = 15.6 Hz, 1H, CHCO), 6.55 (s, 1H, Ph–H), 6.86–6.93 (m, 5H, Ph–H), 7.01(s, 1H, NH), 7.41 (d, J = 7.60 Hz, 2H, Ph–H), 7.55 (d, J = 15.6 Hz, 1H, Ph–CH).

4.2.2.2. (*E*)-3-Methoxy-*N*-(4-(4-(2-methoxyphenyl)piperazin-1-yl)butyl)-cinnamoylamide (1b). Method A, 74% yield, mp: 71–73 °C. ^1H NMR (300 MHz, $CDCl_3$): δ 1.65 (s, 4H, CH_2CH_2), 2.46 (t, J = 7.62 Hz, 2H, 1-Pipera-CH_2), 2.67 (s, 4H, Pipera-H), 3.13 (s, 4H, Pipera-H), 3.42 (t, J = 5.88 Hz, 2H, CH_2CONH), 3.84 (s, 3H, OCH_3), 3.86 (s, 3H, OCH_3), 6.38 (d, J = 15.4 Hz, 1H, CHCO), 6.71 (s, 1H, NH), 6.85–7.08 (m, 7H, Ph–H), 7.22–7.27 (m, 1H, Ph–H), 7.50 (d, J = 15.4 Hz, 1H, Ph–CH). LRMS (CI, *m*/*z*): 423 ($[M+H]^+$, 52%), 261 (100%). HRMS (CI, *m*/*z*): calcd for $C_{25}H_{34}N_3O_3$ 423.2599. Found 423.2512.

4.2.2.3. (*E*)-2-Methoxy-*N*-(4-(4-(2-methoxyphenyl)piperazin-1-yl)butyl)-cinnamoylamide (1c). Method A, 75% yield, mp: 136–138 °C. ^1H NMR (300 MHz, $CDCl_3$): δ 1.65 (s, 4H, CH_2CH_2), 2.49 (t, J = 6.62 Hz, 2H, 1-Pipera-CH_2), 2.70 (s, 4H, Pipera-H), 3.13 (s, 4H, Pipera-H), 3.42 (d, J = 5.15 Hz, 2H, CH_2CONH), 3.82 (s, 3H, OCH_3), 3.86 (s, 3H, OCH_3), 6.38 (d, J = 15.4 Hz, 1H, CHCO), 6.84–6.97 (m, 6H, Ph–H and NH), 6.98–7.03 (m, 1H, Ph–H), 7.26–7.32 (m, 1H, Ph–H), 7.43 (d, J = 7.36 Hz, Ph–H), 7.82 (d, J = 15.4 Hz, 1H, Ph–CH). LRMS (CI, *m*/*z*): 423 ($[M+H]^+$, 13.2%), 178 (100%). HRMS (CI, *m*/*z*): calcd for $C_{25}H_{34}N_3O_3$ 423.2599. Found 423.2519.

4.2.2.4. (*E*)-4-Hydroxy-*N*-(4-(4-(2-methoxyphenyl)piperazin-1-yl)butyl)-cinnamoylamide (1d). Method A, 47% yield; Method B, 76% yield, mp: 124–126 °C. ^1H NMR (300 MHz, $CDCl_3$): δ 1.47 (s, 4H, CH_2CH_2), 2.32 (s, 2H, 1-Pipera-CH_2), 2.94 (s, 4H, Pipera-H), 3.16 (d, J = 5.11 Hz, 2H, CH_2CONH), 3.34 (s, 4H, Pipera-H), 3.76 (s, 3H, OCH_3), 6.37 (d, J = 15.4 Hz, 1H, CHCO), 6.71 (s, 1H, NH), 6.76–6.95 (m, 6H, Ph–H), 7.27 (d, J = 16.1 Hz, 1H, Ph–CH), 7.35 (d, J = 8.82 Hz, 2H, Ph–H), 7.97 (t, J = 5.51 Hz, NH), 9.81(s, 1H, OH). LRMS (CI, *m*/*z*): 410 ($[M+H]^+$, 12.2%), 405 (100%). HRMS (CI, *m*/*z*): calcd for $C_{24}H_{32}N_3O_3$ 410.2444. Found 410.3913.

4.2.2.5. (*E*)-3-Hydroxy-*N*-(4-(4-(2-methoxyphenyl)piperazin-1-yl)butyl)-cinnamoylamide (1e). Method A, 43% yield; Method B, 52% yield, mp: 130–132 °C. ^1H NMR (300 MHz, $CDCl_3$): δ 1.61 (s, 4H, CH_2CH_2), 2.50 (t, J = 6.62 Hz, 2H, 1-Pipera-CH_2), 2.75 (s, 4H, Pipera-H), 3.14 (s, 4H, Pipera-H), 3.36 (t, J = 5.61 Hz, 2H, CH_2CONH), 3.84 (s, 3H, OCH_3), 6.31 (d, J = 15.4 Hz, 1H, CHCO), 6.76–7.03 (m, 7H, Ph–H), 7.16 (t, J = 7.70 Hz, 1H, NH), 7.25 (s, 1H, Ph–H), 7.53 (d, J = 15.4 Hz, 1H, Ph–CH). LRMS (CI, *m*/*z*): 410 ($[M+H]^+$, 20%), 406 (100%). HRMS (CI, *m*/*z*): calcd for $C_{24}H_{32}N_3O_3$ 410.2444. Found 410.3915.

4.2.2.6. (*E*)-2-Hydroxy-*N*-(4-(4-(2-methoxyphenyl)piperazin-1-yl)butyl)-cinnamoylamide (1f). Method A, 36% yield; Method B, 80% yield, mp: 167–169 °C. ^{1}H NMR (300 MHz, $CDCl_3$): δ 1.63 (s, 4H, CH_2CH_2), 2.19 (s, 1H, OH), 2.48 (s, 2H, 1-Pipera-CH_2), 2.73 (s, 4H, Pipera-H), 3.13 (s, 4H, Pipera-H), 3.39 (s, 2H, CH_2CONH), 3.86 (s, 3H, OCH_3), 6.61 (d, J = 15.4 Hz, 1H, CHCO), 6.80–7.01 (m, 7H, Ph–H), 7.17 (t, J = 7.48 Hz, 1H, NH), 7.28–7.39 (m, 1H, Ph–H), 7.91 (d, J = 15.4 Hz, 1H, Ph–CH). LRMS (CI, *m/z*): 410 ([M+H]$^+$, 28%), 137 (100%). HRMS (CI, *m/z*): calcd for $C_{24}H_{32}N_3O_3$ 410.2444. Found 410.3913.

4.3. Synthesis of target tracers

4.3.1. Typical experimental procedure for the radiosynthesis of (*E*)-4,3,2-[^{11}C]methoxy-*N*-4-(4-(2-methoxyphenyl)piperazin-1-yl)butyl-cinnamoylamides (4-[^{11}C]MMC, [^{11}C]1a; 3-[^{11}C]MMC, [^{11}C]1b; 2-[^{11}C]MMC, [^{11}C]1c). The precursor (**1d**, **1e**, or **1f**) (0.6–1.0 mg) was dissolved in CH_3CN (500 μL). To this solution, tetrabutylammonium hydroxide (TBAH) (5 μL, 1 M solution in methanol) was added. The mixture was transferred to a small volume, three-necked reaction tube. [^{11}C]Methyl triflate was passed into the air-cooled reaction tube at −15 to −20 °C, which was generated by a Venturi cooling device powered with 100 psi compressed air, until radioactivity reached a maximum (~3 min), then the reaction tube was heated at 70–80 °C for 2 min. The contents of the reaction tube were diluted with $NaHCO_3$ (1 mL, 0.1 M). This solution was passed onto a C-18 cartridge by gas pressure. The cartridge was washed with H_2O (2 × 3 mL), and the aqueous washing was discarded. The product was eluted from the column with EtOH (2 × 3 mL), and then passed onto a rotatory evaporator. The solvent was removed by evaporation under high vacuum. The labeled product [^{11}C]**1a**, [^{11}C]**1b**, or [^{11}C]**1c** was formulated with saline (1–3 mL), sterile-filtered through a sterile vented Millex-GS 0.22 μm cellulose acetate membrane, and collected into a sterile vial. Total radioactivity was assayed, and total volume was noted. The overall synthesis time was ~20 min. The decay-corrected yield, from $^{11}CO_2$, was 40–65%, and the radiochemical purity was >99% by analytical HPLC.

4.4. PET imaging of the tracers in the Sprague–Dawley female rats

4.4.1. Dynamic IndyPET-II imaging of the tracers 4,3,2-[^{11}C]MMCs in the rats. All animal experiments were performed under a protocol approved by the Indiana University institutional animal care and use committee. The IndyPET-II scanner designed and developed by Rouze and Hutchins[16] was used for these studies. The female Sprague–Dawley rat (250–300 g) was anesthetized with acepromazine (0.2 mg/kg, i.m.) and torbugesic (0.2 mg/kg, i.m.). Dose in the range of 0.5–1.0 mCi of 4-[^{11}C]MMC, 3-[^{11}C]MMC or 2-[^{11}C]MMC was administered intravenously to the rat via the tail vein. The μ-PET images of the tracers were acquired in IndyPET-II scanner by the ordered subsets expectation maximization (OSEM) using six subsets/four iterations for 60 min dynamic scans from a rat post-intravenous injection of 0.5–1.0 mCi of the tracer, and frame durations were defined as 300 s for the entire 3600-s scan.

4.4.2. Image registration and fusion. After sedation, the subject is strapped to a scanning bed, which is mounted on the EVS μ-CT imaging stage for CT image acquisition. Following the CT scan, the bed is moved from the EVS μ-CT imaging stage to the IndyPET-II imaging stage. Both stages have identical mounts with precision pins so that the bed position is reproducible. A six-parameter rigid body registration transform of the PET image to the CT image space is calculated using PET and CT images of a registration phantom consisting of parallel and perpendicular tubes filled with a mixture of [^{18}F]FDG and iodinated contrast agent. Transformation parameters were calculated using an algorithm that finds the ends of the tubes and calculates a geometric transform using the locations of the end points in the two image pairs. This method also provides a measure of fiducial registration error. Typically, the overall fiducial registration error is less than 0.4 mm. The phantom derived registration transformation parameters are applied to the animal CT and PET data sets to register the anatomical and functional image data sets for further evaluation.

4.4.3. Blocking IndyPET-II imaging of the tracers 4,3,2-[^{11}C]MMCs with corresponding cold drugs 4,3,2-MMCs. For the blocking experiments, the rats (250–300 g) were pretreated by intraperitoneal injection with drugs 4,3,2-MMCs (3.0 mg/kg) prior to intravenous injection of corresponding tracers 4,3,2-[^{11}C]MMCs in the tail vein. After tracer administration, the animals were handled as described above.

4.5. Statistical analysis

The uptake differences between control group and blocker group for the tracers 4,3,2-[^{11}C]MMCs, 4-[^{11}C]MMC with 3-[^{11}C]MMC, 4-[^{11}C]MMC with 2-[^{11}C]MMC, and 3-[^{11}C]MMC with 2-[^{11}C]MMC in control group in animals were examined for statistical significance using the Student's *t*-test. A *P*-value less than 0.05 denoted the presence of a statistically significant difference.

Acknowledgments

This work was partially supported by the Indiana 21st Century Research and Technology Fund and the Indiana Genomics Initiative (INGEN) of Indiana University, which is supported in part by Lilly Endowment Inc. The authors would like to thank Winston Baity, Terry McBride, Tanya Martinez, and Kristan Boling for their assistances in animal studies, and Drs. Evan Morris and Karmen Yoder for their helpful advice on PET data analysis. The referee's criticisms and editor's comments for the revision of the manuscript are greatly appreciated.

References and notes

1. Hackling, A.; Ghosh, R.; Perachon, S.; Mann, A.; Holtje, H. D.; Wermuth, C. G.; Schwartz, J. C.; Sippl, W.; Sokoloff, P.; Stark, H. *J. Med. Chem.* **2003**, *46*(18), 3883.

2. Chu, W.; Tu, Z.; McElveen, E.; Xu, J.; Taylor, M.; Luedtke, R. R.; Mach, R. H. *Bioorg. Med. Chem.* **2005**, *13*(1), 77.
3. Vera, D. R.; Eckelman, W. C. *Nucl. Med. Biol.* **2001**, *28*(5), 475.
4. Grunder, G.; Siessmeier, T.; Piel, M.; Vernaleken, I.; Buchholz, H. G.; Zhou, Y.; Hiemke, C.; Wong, D. F.; Rosch, F.; Bartenstein, P. *J. Nucl. Med.* **2003**, *44*(1), 109.
5. Sedvall, G.; Farde, L.; Hall, H.; Halldin, C.; Karlsson, P.; Nordstrom, A. L.; Nyberg, S.; Pauli, S. *Clin. Neurosci.* **1995**, *3*, 112.
6. Olsson, H.; Halldin, C.; Swahn, C. G.; Farde, L. *J. Cereb. Blood Flow. Metab.* **1999**, *19*, 1164.
7. Zhang, M. R.; Haradahira, T.; Maeda, J.; Okauchi, T.; Kawabe, K.; Noguchi, J.; Kida, T.; Suzuki, K.; Suhara, T. *Nucl. Med. Biol.* **2002**, *29*, 233.
8. Lannoye, G. S.; Moerlein, S. M.; Parkinson, D.; Welch, M. J. *J. Med. Chem.* **1990**, *33*, 2430–2437.
9. Fei, X.; Mock, B. H.; DeGrado, T. R.; Wang, J.-Q.; Glick-Wilson, B. E.; Sullivan, M. L.; Hutchins, G. D.; Zheng, Q.-H. *Synth. Commun.* **2004**, *34*, 1897.
10. Yoder, K. K.; Kareken, D. A.; Seyoum, R. A.; O'Connor, S. J.; Wang, C.; Zheng, Q.-H.; Mock, B. H.; Morris, E. D. *Alcohol. Clin. Exp. Res.* **2005**, *29*, 965.
11. Mock, B. H.; Mulholland, G. K.; Vavrek, M. T. *Nucl. Med. Biol.* **1999**, *26*(4), 467.
12. Zheng, Q.-H.; Mulholland, G. K. *Nucl. Med. Biol.* **1996**, *23*(8), 981.
13. Zheng, Q.-H.; Fei, X.; Liu, X.; Wang, J.-Q.; Sun, H. B.; Mock, B. H.; Stone, K. L.; Martinez, T. D.; Miller, K. D.; Sledge, G. W.; Hutchins, G. D. *Nucl. Med. Biol.* **2002**, *29*(7), 761.
14. Fei, X.; Zheng, Q.-H. *J. Liq. Chromatogr. Rel. Technol.* **2005**, *28*, 939.
15. Wang, J.-Q.; Miller, M. A.; Fei, X.; Stone, K. L.; Lopshire, J. C.; Groh, W. J.; Zipes, D. P.; Hutchins, G. D.; Zheng, Q.-H. *Nucl. Med. Biol.* **2004**, *31*(7), 957.
16. Rouze, N. C.; Hutchins, G. D. *IEEE Trans. Nucl. Sci.* **2003**, *50*(5), 1491.
17. Hutchins, G. D.; Rouze, N.; Stone, K. L.; Krishnamurthi, G.; Liang, Y. *J. Nucl. Med.* **2002**, *43*(5 Suppl S), 59P.
18. Luurtsema, G.; Molthoff, C. F.; Schuit, R. C.; Windhorst, A. D.; Lammertsma, A. A.; Franssen, E. J. *Nucl. Med. Biol.* **2005**, *32*(1), 87.